MICROSTRUCTURAL AND MECHANICAL PROPERTIES OF MICROALLOYED STEELS PROCESSED TO SIMULATE THIN SLAB CASTING AND DIRECT ROLLING CONDITIONS

A. I. Fernández, P. Uranga, B. López and J. M. Rodriguez-Ibabe

CEIT and ESII, Pº M. Lardizabal 15, 20018 – San Sebastián, Basque Country (Spain)

ABSTRACT

Plane strain compression tests have been used to simulate Conventional Controlled Rolling (CCR) and Thin Slab Direct Rolling (TSDR) of a Nb and a Nb-Ti microalloyed steel. Reheating at the very high temperature of 1400ºC was used to simulate the TSDR initial conditions, while a lower reheating temperature of 1200ºC was applied in the simulations of conventional CCR process. After deformation and air cooling ferrite+pearlite structures were obtained in both simulations, however, the TSDR simulation exhibited a more heterogeneous microstructure and coarser mean ferrite grain size for both steels than that obtained in the CCR simulation. The conventional tensile properties of the achieved microstructures have been evaluated. Fracture toughness tests (fatigue precracked 3 pb specimens) were performed. The behaviour was completely ductile for both processing routes in the Nb steel, whilst it was found a big difference between both processing routes in the Nb-Ti steel. In the latter the behaviour observed after CCR simulation was ductile, but the TSDR simulation behaviour was ductile-brittle. Fractographic analysis indicates that this different behaviour can be related to the much more heterogeneous grain size distribution present in the microstructure corresponding to the TSDR simulation comparing to the CCR one, and the presence of coarse TiN particles (>1μm). In the TSDR process the big fraction of coarse grains is the microstructural parameter controlling the cleavage fracture when the coarse TiN particles are broken.

INTRODUCTION

From the point of view of mechanical behaviour, grain refinement is considered as the most important procedure to improve simultaneously strength and toughness. This is the main objective of thermomechanical treatments (control rolling) applied to Nb and Nb-Ti steels. Nevertheless, the development of new technologies, as Thin Slab Casting followed by Direct Rolling TSDR, brings about some new microstructural phenomena of the previous steels [1-5]. The most serious problem is the initial austenite grain size, which is much coarser than that obtained after reheating in cold charging processes (effect which is more marked for these steels microalloyed with Nb or Ti, because these elements are inhibitors of austenite grain growth during reheating previous to cold charging). Moreover, the refinement of this coarse as-cast microstructure by static recrystallization during subsequent rolling is limited because a much smaller amount of strain than in the conventional hot rolling is usually provided after casting near-net-shape slabs. Thus, as it is widely reported [1-5] in the case of TSDR microalloyed processed steels, the final microstructure might be ineffectively refined, resulting in a mixed ferrite grain size with a wide range of grain sizes than can impair their toughness behaviour.

In this study the microstructural and mechanical properties of a Nb and a Nb-Ti microalloyed steel, deformed by plane strain compression after reheating at 1200 or 1400ºC in order to simulate CCR or TSDR processes respectively, have been analyzed. Their fracture micromechanisms in each condition have also been studied and related to microstructural inhomogeneities.

MATERIAL AND EXPERIMENTAL TECHNIQUES

The chemical compositions (in wt %) of the steels used are listed in Table 1. Plane strain compression tests were used for simulate plate rolling. The geometry of the specimen employed for each type of test is indicated in Table 2. After soaking for 15 min at different temperatures, 1200ºC and 1400ºC for CCR and TSDR simulations respectively, three deformation passes were applied at a constant strain rate of $10s^{-1}$ during the continuous cooling of the specimen. The values of pass temperatures and applied deformations for each condition are summarised in Table 2. After the last deformation, the specimens were air cooled (≈ 2ºC/s and ≈ 3ºC/s in 90x50x20 and 90x25x20 sized specimens, respectively).

TABLE 1
CHEMICAL COMPOSITIONS OF THE STEEL (WT %)

Steel	C	Mn	Si	S	P	Al	Nb	Ti	N
Nb	0.1	1.42	0.31	0.008	0.018	0.039	0.035	-	0.0053
Nb-Ti	0.07	0.62	0.012	0.006	0.011	0.053	0.034	0.067	0.0043

Microstructural characterization was carried out on longitudinal sections cut from the plane strain compression specimens and after etching with nital the microstructure was analyzed by optical microscopy. Tensile and J_{Ic} tests (three point bending, ASTM E813 standard, with a thickness B = 6 or 9 mm and a width W = 12 or 18 mm) were performed on specimens machined from the deformed samples. The fracture surfaces of the 3 pb specimens were examined in a Philips XL30 SEM.

TABLE 2
PLANE STRAIN COMPRESSION TEST PARAMETERS

Steel	Schedule	Sample Geometry	$T_{reh.}$ (ºC)	Pass 1		Pass 2		Pass 3	
				T (ºC)	ε	T (ºC)	ε	T (ºC)	ε
Nb	A	90x50x20	1200	1145	0.44	954	0.46	898	0.46
	B	90x50x20	1400	1200	0.40	950	0.38	900	0.62
	C	90x25x20	1400	1150	0.43	950	0.43	900	0.40
Nb-Ti	D	90x50x25	1200	1175	0.25	952	0.35	902	0.35
	E	90x50x25	1400	1200	0.25	950	0.35	900	0.35

RESULTS

Microstructural Characterization

The preheating temperature of 1200ºC has been chosen for laboratory simulations of CCR processes. The preheating temperature of 1400ºC, which leads to a coarser initial grain size previous to deformation and also to a higher amount of microalloying elements in solid solution, has been chosen for the simulations of TSDR processes. The austenite grain sizes obtained for each condition are listed in Table 3. The resulting microstructures obtained in plane strain compression tests for both processing routes (CCR and TSDR) are shown in Figure 1 for the Nb steel and in Figure 2 for the Nb-Ti steel. For each microstructure the constituent volume fractions and the mean ferrite grain size d_α have been determined. The results are summarised as well in Table 3. For both steels the principal constituent is polygonal ferrite. The Nb steel

deformed by Schedule C presents a higher volume fraction of pearlite, 23% comparing to about 10% obtained in Schedules A and B. This difference is associated to the higher cooling rate derived from the smaller dimension of the plane strain specimen. In this case there is also a small fraction of acicular structure (4%). However, in the case of the Nb-Ti steel the measured ferrite fraction is quite similar for all the deformation conditions, and the amount of pearlite very small (< 2%).

TABLE 3
MICROSTRUCTURAL CHARACTERIZATION OF PLANE STRAIN COMPRESSION TESTS

Steel	Schedule	$T_{reh.}$ (ºC)	D_o (μm)	d_α (μm)	f_α (%)	$f_{pearlite}$ (%)	$f_{acic.\ struc.}$ (%)
Nb	A	1200	192	5.8 ± 0.3	89 ± 2	11 ± 2	-
	B	1400	727	8.9 ± 0.4	90 ± 2	10 ± 2	-
	C	1400	727	7.4 ± 0.4	73 ± 3	23 ± 2	4 ± 1
Nb-Ti	D	1200	109	8.2 ± 0.3	98.2 ± 0.8	1.8 ± 0.8	-
	E	1400	550	9.7 ± 0.5	99.0 ± 0.6	1.0 ± 0.6	-

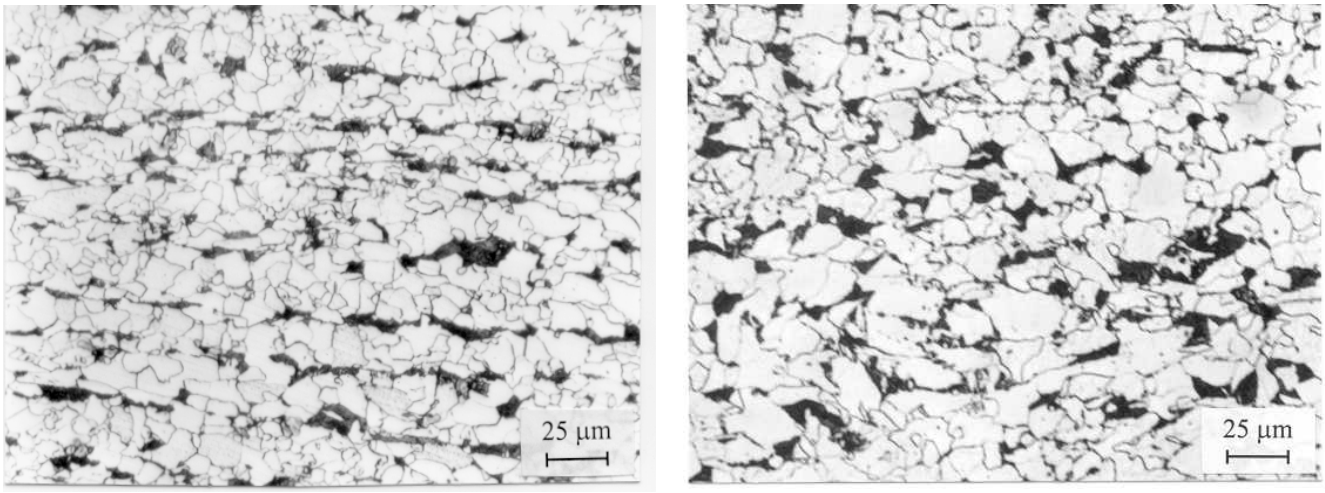

(a) (b)

Figure 1: Microstructure of Nb steel obtained from plane strain compression tests after soaking at: (a) 1200ºC (Schedule A); and (b) 1400ºC (Schedule C).

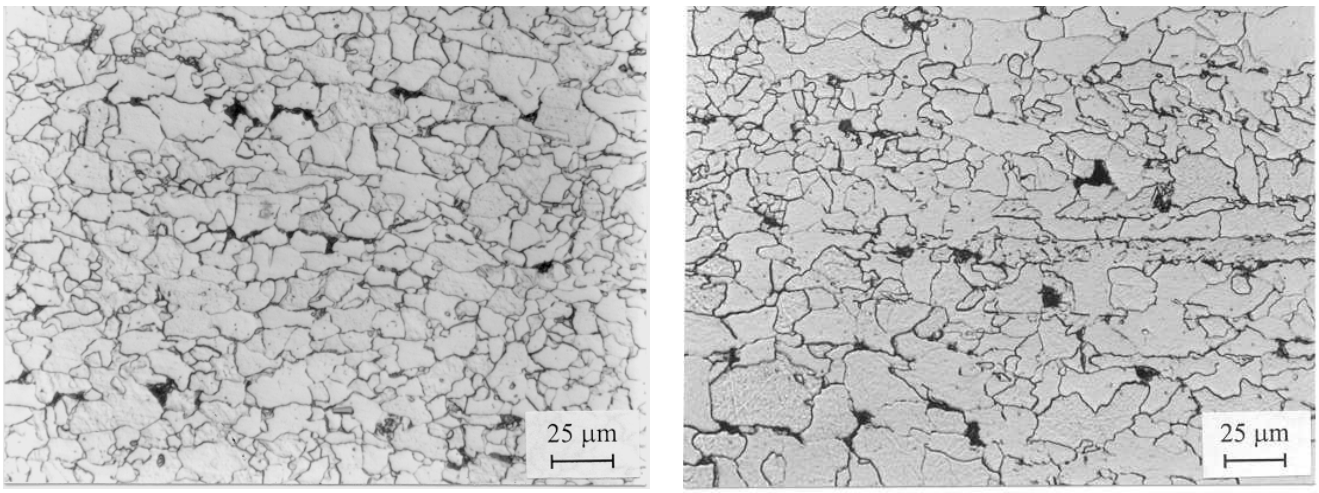

(a) (b)

Figure 2: Microstructure of Nb-Ti steel obtained from plane strain compression tests after soaking at: (a) 1200ºC (Schedule D); and (b) 1400ºC (Schedule E).

It is worth emphasising that in both steels, after deformation and transformation to room temperature the resulting mean ferrite grain sizes are finer after the CCR simulations (see Table 3). Additionally it has been observed that the TSDR simulations lead to more heterogeneous microstructures than those obtained in the

case of CCR ones. From Figures 1(b) and 2(b) the presence in the microstructure of very coarse grains coexisting with much finer ones is clearly observed. These observations are confirmed by the distributions of the ferrite grain sizes shown in Figure 3 and Figure 4 for the Nb and the Nb-Ti steel respectively. The spread of the distribution to larger grain sizes for both steels in TSDR processed samples is clearly evident, being more notorious for the Nb-Ti steel.

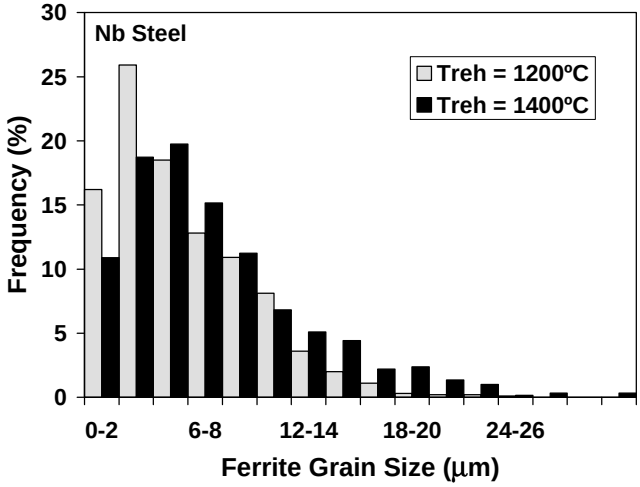

Figure 3: Ferrite grain size distributions of Nb steel preheated at 1200ºC and 1400ºC (Schedule C).

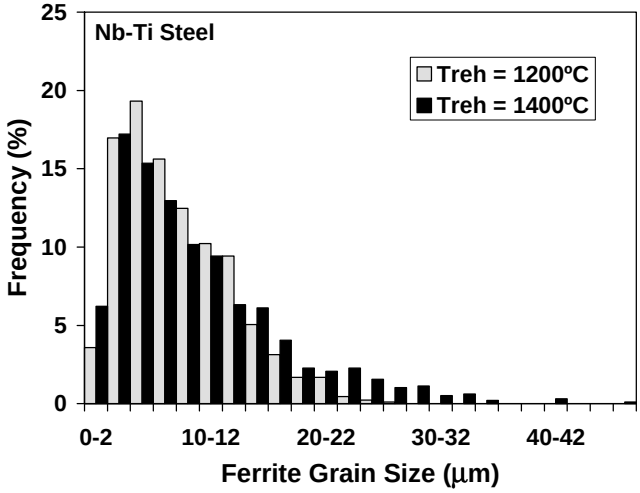

Figure 4: Ferrite grain size distributions of Nb-Ti steel preheated at 1200ºC and 1400ºC.

Mechanical Characterization

The tensile properties ($\sigma_{0.2\%}$, σ_{max}, UTS and R.A.) determined for the different microstructures in both steels are listed in Table 4. Each value corresponds to the mean results obtained from, at least, 2 specimens. Both steels show similar tensile properties after simulations of both processing routes in specimens cooled at the same cooling rate (equal dimensions). A different behaviour is observed for the Nb steel deformed by Schedule C. In this case, as it was mentioned before, the higher cooling rate due to a smaller sized specimen leads to an increase in the final microstructure of pearlite and acicular products. As a result an increase of strength is obtained in this case.

From the point of view of fracture toughness tests, it was observed that the Nb steel soaked at 1200ºC presented a completely ductile behaviour, both, at room temperature and at –20ºC. Similarly, after soaking at 1400ºC (Schedule C), a ductile behaviour was observed at – 20ºC. On the other hand, the Nb-Ti steel soaked at 1200ºC showed a ductile behaviour at – 20ºC, while this steel, after soaking at 1400ºC, exhibited at the same test temperature a behaviour corresponding to the lower part of the ductile-brittle transition, with a very small ductile propagation (<< 0.2 mm). In the last case from the load-displacement curve the J_c value,

worked out using the proposed European ESIS procedure, was determined. The value obtained was 17.3 $kPa \cdot m$, which corresponds to a value of K_c = 64 $MPa \cdot \sqrt{m}$. For the rest of the investigated conditions, due to the small specimen dimensions, it was not possible to obtain the standard J_{Ic} value, but values of J_Q higher than 115 $kPa \cdot m$ have been obtained.

TABLE 4
MECHANICAL PROPERTY CHARACTERIZATION OF SPECIMENS DEFORMED BY PLANE STRAIN COMPRESSION TESTS

Steel	Schedule	T_{reh} (ºC)	$\sigma_{0.2\%}$ (MPa)	UTS (MPa)	σ_{max} (MPa)	R.A. (%)
Nb	A	1200	387	535	628	68
	B	1400	384	520	588	71
	C	1400	460	597	690	73
Nb-Ti	D	1200	344	440	502	76
	E	1400	343	447	501	73

Figure 5 shows some examples of the ductile behaviour at – 20ºC of the microstructure corresponding to the Nb steel soaked at 1200ºC and at 1400ºC (Schedule C). In all these cases voids of different sizes are clearly evident. An example of the ductile propagation that has taken place in the case of the Nb-Ti steel reheated at 1200ºC and tested at - 20ºC is shown in Figure 6. In this case, inside one of the voids a coarse broken TiN particle can be observed (see the detail in Figure 6b). On the other hand, in Figure 7 it can be observed a coarse TiN particle, which has been identified as the origin of brittle fracture, in a specimen of the Nb-Ti steel reheated at 1400ºC and tested at –20ºC. Other coarse broken TiN particles have also been observed in the fracture surface promoting secondary cleavage fractures.

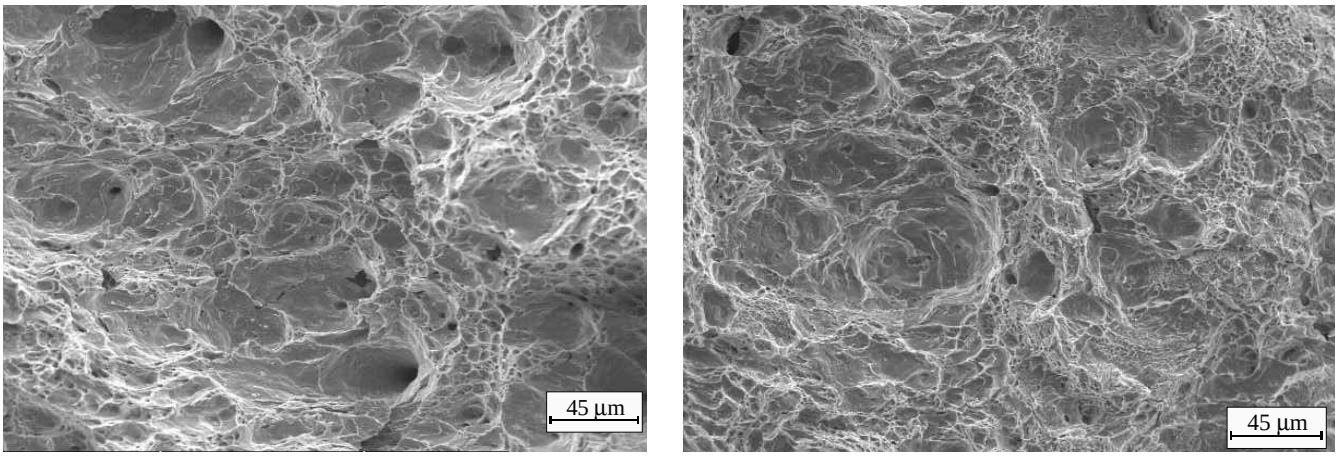

(a) (b)

Figure 5: Ductile behaviour at – 20ºC of Nb steel soaked at: (a) 1200ºC; and (b) 1400ºC (Schedule C).

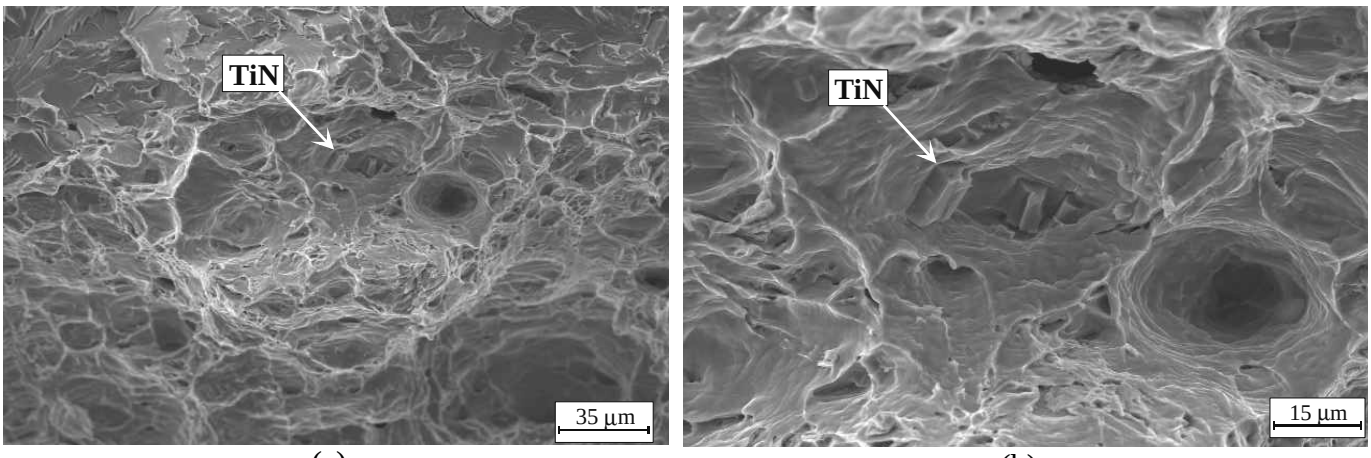

(a) (b)

Figure 6: Ductile behaviour at – 20ºC of the microstructure presented for Nb-Ti steel soaked at 1200ºC: (a) general view; and (b) detail showing a coarse broken TiN particle inside a void.

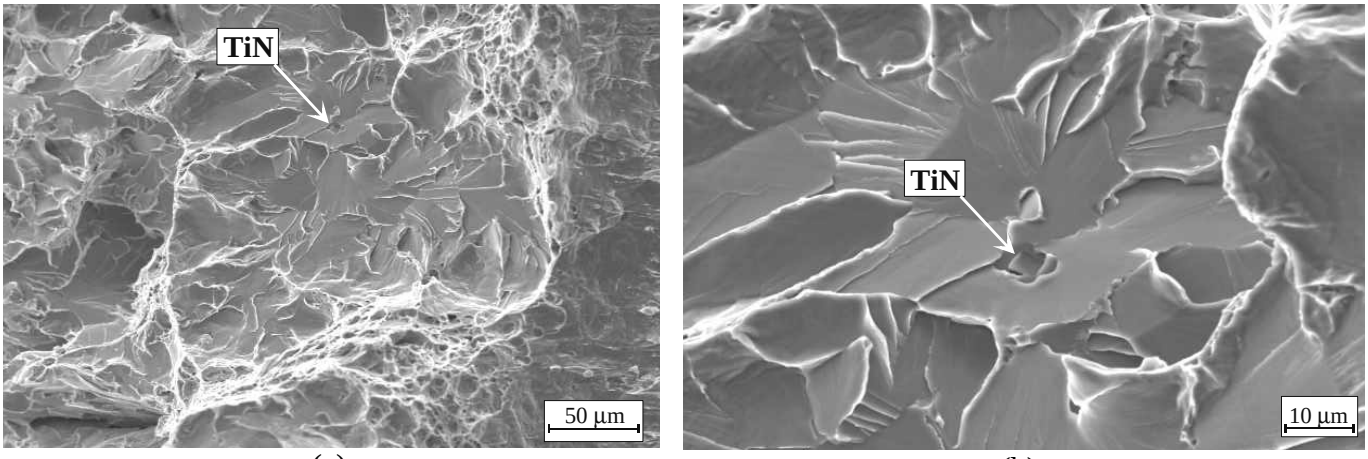

(a) (b)

Figure 7: Origin of the brittle fracture presented at – 20ºC for the Nb-Ti steel soaked at 1400ºC): (a) general view; and (b) detail of the broken fracture initiator particle.

DISCUSSION

From the previous results it has been shown that after deforming the large austenite grains, typical of TSDR processes, the resulting microstructures are coarser and much more heterogeneous than those obtained for the lower austenite grain sizes, characteristic of as-reheated austenite in CCR processes. A great heterogeneity in the microstructure was also previously detected by other authors [1-5], though, on the contrary to that observed in the present work, some of them [1,2] obtained a finer mean ferrite grain size in TSDR simulations than in CCR ones.

The static recrystallization kinetics of the present steels was analyzed in a previous work for a wide range of initial austenite grain sizes [6]. Taking into account the static recrystallization equations obtained in that work, it can be deduced that for all the deformation conditions used here (see Table 2), the materials are able to recrystallize after the first pass, but not after subsequent passes. In all cases the temperatures of pass 2 and 3 are below the non-recrystallization temperature determined for the steels [7], which means that strain is accumulated in the austenite during deformation at these low temperatures. The difference between both processing routes is that strain accumulates in the austenite on a very different recrystallized grain size, much coarser and heterogeneous in the case of TSDR simulations [8]. This means that for the large initial austenite grain size, the applied deformation schedules have been insufficient to reach an homogenous austenite microstructure before transformation. In contrast, the ferrite grain refinement in CCR simulations is mainly due to the lower initial grain size.

The lower average ferrite grain size obtained after CCR simulations would imply higher tensile properties, in comparison to TSDR ones. It has been observed that the tensile data obtained for the Nb-Ti steel after both processing routes are very similar, in spite of the differences in ferrite grain size. The same occurs for the Nb steel after deformation by Schedules A and B. This result can only be explained if the softening caused by the presence of a coarser ferrite grain size is compensated by a larger contribution of the strengthening due to precipitation in TSDR products. A higher tendency to precipitate during transformation after this processing route is expected because a higher quantity of microalloying elements is in solid solution in comparison to the conventional CCR route leading to an increase in the driving force for precipitation [1-3]. In the case of the Nb steel deformed by Schedule C, the difference of 60 MPa in tensile properties can be attributed to the higher pearlite and acicular volume fraction, as much as 27% comparing to the 10% obtained after Schedule B.

In relation to toughness, the results have shown that the Nb steel has for both processing routes a completely ductile behaviour at – 20ºC, meanwhile the behaviour of the Nb-Ti steel is ductile for CCR simulation but is ductile-fragile for TSDR one. This different toughness behaviour in the Nb-Ti steel could be related to the more heterogeneous ferrite grain size in the case of TSDR simulation than in the CCR one (see Figure 2 and

Figure 4). Nevertheless, this reason is not sufficient to explain the toughness difference, taking into account that a similar heterogeneous microstructure in the Nb steel does not lead to lower toughness. In consequence, to analyze this change it is required to consider the micromechanisms intervening in the brittle process.

The process of brittle cleavage fracture has been attributed to the nucleation of a microcrack followed by its propagation into the surrounding matrix. This process can be divided into three different steps [9,10]. In the first step a microcrack nucleates in an appropriate microstructural feature (a grain-boundary carbide, a non-metallic inclusion…) which fractures easily in a brittle manner. The second step consists of the propagation of the microcrack to the surrounding matrix, given that the local stress exceeds a certain critical value. The third critical step, for crack progression through the matrix, arises at high angle boundaries which act as obstacles and force the microcrack to change the microscopic plane of propagation in order to accommodate the new local crystallography. The step necessary to cleavage fracture (Step 1) in which a brittle particle breaks originating a microcrack depends on brittle particle nature and its distribution size and volume fraction. Step 2 and 3 depend on microstructural parameters.

For the Nb-Ti steel, in both simulations, broken TiN coarse particles (> 1μm) can be observed in the cleavage surfaces. These particles have been precipitated during the solidification of the steel and the subsequent soaking at 1200ºC or 1400ºC has not been able to dissolve them. It has been widely reported that the microcraks nucleated in these broken TiN coarse particles [11,12] can promote cleavage fracture initiation in the brittle and in the brittle-ductile transition regions. Nevertheless, at equal quantity and distribution of these particles in the matrix, microstructural parameters control the toughness behaviour of the steel. For low carbon steels with predominantly ferrite microstructures, the ferrite grain size corresponds to the cleavage facet size, and as a consequence, the ferrite grain boundary controls Step 3 [13]. In CCR simulation these broken TiN coarse particles can be observed inside the voids (see Figure 6), meanwhile in TSDR simulation the origin of the cleavage fracture and also the origin of several secondary cleavages fractures are associated with these cracked particles (see Figure 7). Therefore, the microcracks initiated in a brittle manner on coarse TiN particles (step 1 of cleavage process) have been stopped at particle-matrix interface (step 2) in the case of CCR simulation, giving place to ductile fracture modes with void formation. On the other hand, the coarser and heterogeneous microstructure presented in the TSDR simulation has promoted the propagation of the microcracks to the ferrite matrix (step 2) taking place a catastrophic propagation to failure (step 3). Thus, an improvement of toughness can be achieved only if a well-refined microstructure is obtained, as it occurs in the case of reheating at 1200ºC.

A similar behaviour was observed by other authors [11-12,14] for a medium carbon steel in which a more heterogeneous microstructure was responsible for poor toughness values, suggesting also that refined microstructures are able to stop the microcracks initiated in a brittle manner on coarse particles, giving place to ductile fracture modes and, in consequence, improved toughness. The coarse facets (see Figure 8) observed in the initiation zone of the cleavage fracture confirm this behaviour.

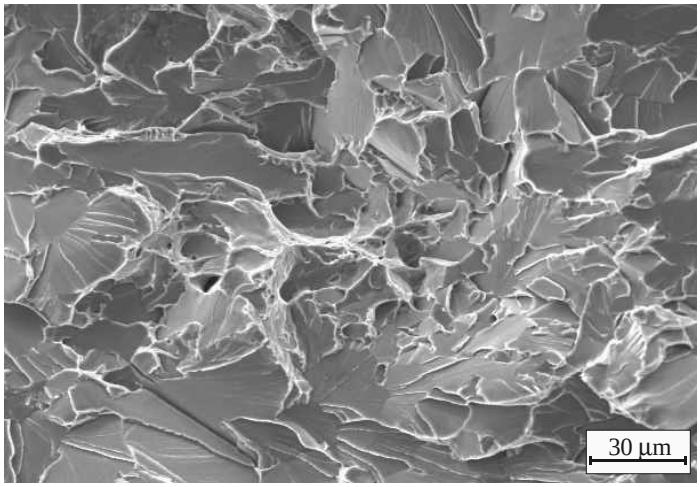

Figure 8: Cleavage fracture surface of 3 pb specimen tested at – 20ºC for the Nb-Ti steel soaked at 1400ºC. Coarse facets can be identified.

The absence of the deleterious coarse TiN particles in the Nb steel has made that, in spite of the heterogeneous microstructure presented in TSDR simulation, ductile behaviour is observed at – 20ºC. However, possibly, as it was found by Kamada et al. [3], for a Nb microalloyed steel the inhomogenous microstructure achieved in TSDR simulations will probably lead to a deterioration effect in the brittle–ductile transition temperature.

Conclusions

- TSDR simulations of Nb and Nb-Ti microalloyed steels have produced in all cases coarser and more heterogeneous microstructures than simulations of conventional CCR processes, due probably to an insufficient refinement of the coarse initial austenite grain size during hot working.

- The combination of an heterogeneous microstructure resulting from the TSDR process with the presence of coarse TiN particles (> 1μm) in the Nb-Ti microalloyed steel is responsible for the brittle-ductile behaviour shown by this steel at –20ºC, in contrast to the ductile behaviour shown by the Nb-steel at the same test temperature. At the same temperature the Nb-Ti steel deformed by CCR processing route shows a completely ductile behaviour. In the latter the finer and more homogeneous ferrite microstructure prevents the propagation of the microcracks generated on TiN particles to the ferrite matrix.

Acknowledgements

Part of the results presented in this work carried out under ECSC contract nº 7210-CA/936 and under a Spanish CICYT research program MAT96-2580-CE. P. U. gratefully acknowledges a research grant from the Basque Government.

References

1. Frawley, L.D., Priestner, R. and Hodgson, P.D. (1997). In: *Int. Conf. THERMEC'97*, pp. 2169-2175, Chandra, T. and Sakai, T. (Eds). TMS, Warrendale.
2. Gibbs, R.K., Peterson, R. and Parker, B.A. (1992). In: *Int. Conf. Proccesing, Microstructure and Properties of Microalloyed Steels*, pp. 201-207, Van Tyne, C.J., Krauss, G. and Matlock, D.K. (Eds). ISS-AIME, Pittsburg, PA.
3. Kamada, Y., Hashimota, T. and Watanabe, S. (1990) *ISIJ Int.* **30**, 241.
4. Priestner, R. and Zhou, C. (1995) *Ironmaking and Steelmaking* **22**, 326.
5. Kunishige, K. and Nagao, N. (1989) *ISIJ Int.* **29**, 940.
6. Fernández, A.I., Uranga, P., López, B. and Rodriguez-Ibabe, J.M., to be published in *ISIJ International.*
7. Abad, R. (1999) Ph. D. Thesis, ESII, Universidad de Navarra, S. Sebastián, Spain.
8. Fernández, A.I. Ph. D. Thesis, ESII, Universidad de Navarra, S. Sebastián, Spain, in progress.
9. McMahon, C. J. and Cohen, M. (1965) *Acta Metall.* **13**, 591.
10. Knott, J.F., (1992). In: *Reliability and Structural Integrity of Advanced Materials, ECF9*, **2**, pp. 1375-1400, Sedmak, S. et al. (Eds). EMAS.
11. San Martín, J.I., Linaza, M.A., Rodriguez-Ibabe, J.M. and Fuentes, M. (1997). In: *Int. Conf. THERMEC'97*, pp. 265-271, Chandra, T. and Sakai, T. (Eds). TMS, Warrendale.
12. Linaza, M.A., Romero, J.L., Rodriguez-Ibabe, J.M. and Urcola, J.J. (1996). In: *Microalloyed Bar and Forging Steels*, pp. 311-325, Van Tyne, C.J., Krauss, G. and Matlock, D. K. (Eds). TMS, Warrendale.
13. Boronat, M., (1997) Internal report, CEIT, S. Sebastián, Spain.
14. Linaza, M.A., Rodriguez-Ibabe, J.M. and Urcola, J.J. (1997) *Fatigue Fract. Eng. Mater. Struc.* **20**, 619.